

TIME-HARMONIC CURRENT DISTRIBUTION ON CONDUCTOR GRID IN HORIZONTALLY STRATIFIED MULTILAYER MEDIUM

P. Sarajčev, S. Vujević^{*}, and D. Lovrić

Faculty of Electrical Engineering, Mechanical Engineering and Naval Architecture, University of Split, Ruđera Boškovića 32, Split HR-21000, Croatia

Abstract—This paper presents a novel time-harmonic electromagnetic model for determining the current distribution on conductor grids in horizontally stratified multilayer medium. This model could be seen as a basis of the wider electromagnetic model for the frequency-domain transient analysis of conductor grids in multilayer medium. The total number of layers and the total number of conductors are completely arbitrary. The model is based on applying the finite element technique to an integral equation formulation. Each conductor is subdivided into segments with satisfying the thin-wire approximation. Complete electromagnetic coupling between segments is taken into account. The computation of Sommerfeld integrals is avoided through an effective approximation of the attenuation and phase shift effects. Computation procedure for the horizontally stratified multilayer medium is based on the successful application of numerical approximations of two kernel functions of the integral expression for the potential distribution within a single layer, which is caused by a point source of time-harmonic current. Extension from the point source to a segment of the earthing grid conductors is accomplished through integrating the potential contribution due to the line of time-harmonic current source along the segments axis.

1. INTRODUCTION

Grounding grid analysis still attracts significant attention from researchers around the world, which could be readily observed from the truly voluminous work published on this subject. It could be asserted

Received 8 April 2011, Accepted 26 May 2011, Scheduled 3 June 2011

^{*} Corresponding author: Slavko Vujević (slavko.vujevic@fesb.hr).

that significant attention is dedicated to the aspects associated with transient grounding grid behavior, as well as on those various aspects of electromagnetic compatibility, again associated with grounding systems performance during both short circuits and lightning surge transients [1].

Generally speaking, according to the treatment of the accompanying electromagnetic field formulation, electromagnetic methods could be classified into two large groups. The first group of methods are the so-called quasi-static methods, which are based on the time-harmonic current energization and ignore attenuation and phase shift effects [2–4]. Applicability of these methods is limited to low frequency, which is adequate for the nominal frequency applications, e.g., single-pole short circuit grounding grid analysis. Second group of methods involve a full electromagnetic field approach, by solving a set of Maxwell equations [5–10]. Numerical methods based on the full electromagnetic theory approach, which rigorously treat boundary layers and numerically solve Sommerfeld integrals, are still mainly limited to homogeneous earth models [5–7] because of their complexity. Only recently, they were expanded to include the two-layer earth models, e.g., [8, 9]. Here, accompanying time-harmonic current source involves attenuation and phase shift effects, which could be rigorously incorporated [5] or approximated in some way [11]. These methods could treat high-frequency phenomena associated with various sophisticated grounding grid analysis. In case of approximate incorporation of attenuation and phase shift effects, upper frequency of applicability should be determined. It depends, in turn, on the quality of the approximation itself. Methods involving attenuation and phase shift effects have wider applicability and higher accuracy, but, at the same time, they are more computer-intensive from the point of view of CPU usage.

A good general presentation and mutual comparison of different numerical methods available for the grounding grid analysis is presented in [1]. Furthermore, some general considerations on grounding systems modeling for high frequencies and transients could be found in [12]. It needs to be stated that contrary to the vast number of simulation oriented papers, there is a great deficiency of carefully documented papers concerned with experimental works on transient grounding grid behavior. Noteworthy exemptions to this rule are given in, e.g., [13–15].

The first step in the process of grounding system electromagnetic model development — regardless of the employed medium model — can be seen in the determination of current distribution on that system of conductors. With known current distribution one can subsequently determine the potential distribution in any point on

and around the conductor grid. Especially important is a potential distribution on the ground surface from which dangerous voltages directly follow. Furthermore, electric and magnetic field distributions can be obtained once the current distribution on the conductor grid is known. Especially important is the electromagnetic field distribution in the air. Introduction of the Fourier transform would facilitate scrutiny of the conductor grid transient behavior [1].

This paper presents a novel numerical method for the analysis of current distribution on conductor grid in horizontally stratified multilayer medium, which is consisted of air and arbitrary number of soil layers. This mathematical representation has a fundamental physical background regarding the behavior of current while passing through earth (e.g., soil resistivity changes with depth as current passes through different layers of soil, sediments and rock). This model could be seen as a basis of the wider electromagnetic model for the frequency-domain transient analysis of conductor grids in multilayer medium.

Electromagnetic model is based on the application of the finite element technique (FET) on the integral problem formulation, which is laid out in the frequency domain, following a full electromagnetic theory approach. Well-known Galerkin - Bubnov method is employed in the FET procedure, combined with a thin-wire approximation of the grounding conductors. Grounding conductors could be arbitrarily positioned in regard to the earth surface, within arbitrary soil layer, even penetrating the earth surface and extending into the air. Complete electromagnetic coupling between grounding grid conductors has been taken into account. Electromagnetic model additionally utilizes an original numerical algorithm for approximating the potential distribution of a time-harmonic current point source in horizontally stratified multilayer medium [11], in order to account for the heterogeneous soil.

The efficiency of the computation procedure for a time-harmonic current point source is based on the successful application of numerical approximations of two kernel functions of the integral expression for the potential distribution within a single layer of the medium model. This is in fact congruous to the approximations of appropriate Green's functions, which are in fact kernel functions of the integral expression for the potential distribution due to unit current point source in multilayer medium. Numerical approximation of the kernel functions of the integral expression for the potential distribution is carried out according to the fixed image method [1,11], which is numerically efficient and stable.

This, in combination with the approximation of the attenuation and phase shift effects, which avoids formation and subsequent

numerical solution of Sommerfeld integrals, makes here proposed procedures extremely numerically efficient. Sommerfeld integrals are known to be numerically ill-behaved and very difficult to solve. Apart from that, numerical solution of Sommerfeld integrals is very time consuming, from the point of view of CPU time. This is the main reason why many researchers tend to avoid them during the course of the development of methods for grounding grid analysis.

Hence, due to the above mentioned procedures, here proposed mathematical model assures high numerical efficiency, which makes this method well suited for the subsequent transient solution, based on the Fourier transform.

Determining the upper frequency of model applicability is a necessary step in the development procedure. This is true for every frequency-domain grounding grid model, especially those which use a quasi-static approximation of the electromagnetic field theory. Due to the fact that hereafter presented electromagnetic model introduces approximations of the attenuation and phase shift effects, its upper frequency of applicability needs to be established. This will be carried out in this paper, by comparing results produced by here presented model with those obtained with the so-called full-wave electromagnetic model.

2. DISCONNECTED SEGMENTS IN MULTILAYER MEDIUM

The first layer of the horizontally stratified multilayer medium is air, while other layers represent multilayer earth model. The total number of layers is completely arbitrary. Conductors could be positioned in any layer of the horizontally stratified multilayer medium, including the air. Using the FET, each conductor is subdivided into segments by satisfying the thin-wire approximation at the same time [11].

Current of the ks -th segment consists of two separate parts: a) longitudinal segment current, which, according to the thin-wire approximation, flows along the segment axis; this current is approximated by a constant, whose value is equal to its average value, b) transversal (leakage) segment current, which leaks uniformly from the segment surface into the surrounding medium; this current is presented with a time-harmonic current line source, positioned along the segment axis.

Let the total number of segments be denoted by N_s . In the first step, all segments, which are electromagnetically coupled, must be disconnected because longitudinal and transversal systems of equations can be created only for disconnected segments. In the second step,

using the FET assembling procedure, disconnected segments will be mutually connected in global nodes. According to the FET terminology, all disconnected segments form a single finite element (local system), whereas connected segments form a global system.

Each disconnected segment has two local nodes. Because of simplicity, the arbitrary ks -th segment has a starting local node denoted by ks and ending local node denoted by $Ns + ks$ (Figure 1). Figure 1 graphically depicts the ks -th segment current separation, along with adopted current notations, subsequently used throughout this paper. The total nodal current entering the ks -th local node \bar{I}_{ks}^n is equal to the sum of the longitudinal $\bar{I}_{ks}^{n\ell}$ and transversal \bar{I}_{ks}^{nt} nodal currents entering the ks -th local node. The same applies for $Ns + ks$ local node.

In accordance with the afore-mentioned, in the numerical model, the transversal nodal currents are equal to the half of the transversal segment current. In other words, half of the segment transversal (leakage) current is transferred into each of the two segment local nodes (Figure 1). The longitudinal segment currents are denoted \bar{I}_{ks}^ℓ , whereas the transversal segment currents are denoted \bar{I}_{ks}^t .

Graphical representation of the horizontally stratified multilayer medium model is given in Figure 2. Let $\bar{\gamma}_1$ denote a complex wave propagation constant of the air, while $\bar{\gamma}_2, \bar{\gamma}_3, \dots, \bar{\gamma}_n$ represent complex wave propagation constants of the earth layers (Figure 2). Complex wave propagation constant of arbitrary p -th medium model layer can be expressed as:

$$\bar{\gamma}_p = j\omega\mu_0 \cdot \bar{\kappa}_p = j\omega\mu_0 \cdot (\sigma_p + j\omega\varepsilon_0\varepsilon_{rp}) \tag{1}$$

where j is the imaginary unit, $\omega = 2 \cdot \pi \cdot f$ is the circular frequency, f is frequency, μ_0 is the medium permeability which is equal to permeability of the vacuum, σ_p is the electrical conductivity of the p -th medium model layer, ε_0 is the permittivity of the vacuum, ε_{rp} is

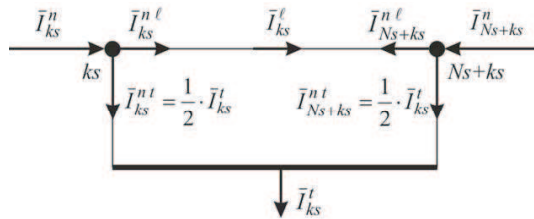


Figure 1. Separation of current into its longitudinal and transversal components.

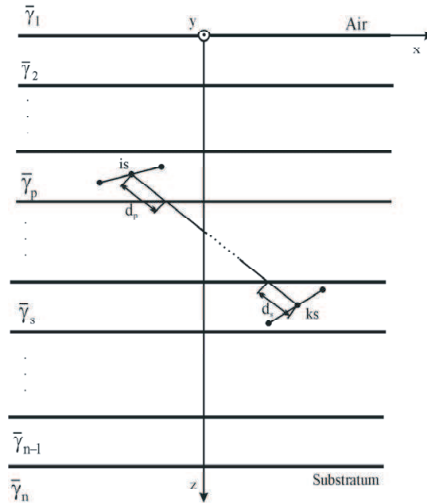


Figure 2. Approximation of the attenuation and phase shift effects.

the relative permittivity of the p -th medium model layer and $\bar{\kappa}_p$ is the complex electrical conductivity of the p -th medium model layer.

3. APPROXIMATION OF THE ATTENUATION AND PHASE SHIFT EFFECTS

Treatment of the segments in horizontally stratified multilayer medium is derived from the theory of time-harmonic current point source in horizontally stratified multilayer medium [11]. It needs to be accentuated here that the efficiency of the solution to the problem of grounding segments in horizontally stratified multilayer medium is bounded by the efficiency of the underlying solution to the problem of current point source in the same medium [1, 11].

Attenuation and phase shift effects in horizontally stratified multilayer medium have been efficiently approximated by the introduction of a complex attenuation–phase shift factor. In such a way Sommerfeld integrals are completely avoided and majority of integrals in the expressions for longitudinal and transversal self and mutual impedances could be analytically solved [16, 17].

Values of the complex attenuation–phase shift factors are computed in two different ways in respect to the expressions involving self segment impedances and expressions involving mutual segment impedances. Figure 2 graphically depicts two arbitrary segments in horizontally stratified multilayer medium.

For the expressions involving self segment impedances, complex attenuation-phase shift factor is computed according to the following equation:

$$\bar{f}_{ks,ks} = 1 + \frac{\int_{\Gamma_{ks}^s} \int_{\Gamma_{ks}} \frac{e^{-\bar{\gamma}_s \cdot R} - 1}{R} \cdot d\ell_{ks} \cdot d\ell_{ks}^s}{\int_{\Gamma_{ks}^s} \int_{\Gamma_{ks}} \frac{1}{R} \cdot d\ell_{ks} \cdot d\ell_{ks}^s} \quad (2)$$

where $\bar{\gamma}_s$ is a complex wave propagation constants of the s -th medium model layer in which ks -th segment is located, R is the distance between the field point and a source point, Γ_{ks} is the path of integration along the segment axis and Γ_{ks}^s is the path of integration along the curve on segment surface, which is parallel to the segment axis. Double integral in the nominator of expression (2) can be solved by employing the integration routine based on double numerical integration with a seven point Gauss Legendre quadrature [16, 17]. Double integral in the denominator of expression (2) has a rather well-known analytical solution [16, 17].

For the expressions involving mutual segment impedances, complex attenuation-phase shift factor between the is -th segment located in the p -th medium model layer and the ks -th segment located in the s -th medium model layer (according to Figure 2) is computed according to the following expression:

$$\bar{f}_{is,ks} = e^{-S} ; \quad S = \sum_{k=bl}^{el} \bar{\gamma}_k \cdot d_k \quad (3)$$

where $bl = \min\{p, s\}$, $el = \max\{p, s\}$. Each penetration of the medium layer with a fictitious line connecting middle points of the segments, augments the summation number in (3). Distances d_k in the above expression could be easily obtained from the analytical geometry in three-dimensional (3D) space. Therefore, attenuation and phase shift effects between two arbitrary segments in multilayer medium are in fact approximated by the complex attenuation-phase shift factor inherent between middle points of these two segments in 3D space. Hence, thus derived attenuation-phase shift factor (3) takes into account all the physical properties of the medium model layers, involved between segments under consideration [11].

4. SYSTEM OF LINEAR EQUATIONS FOR LONGITUDINAL SEGMENT CURRENTS

In FET terminology, as previously mentioned, segment current has been divided into two separate parts: longitudinal and transversal

current (Figure 1). Hence, two separate sets of systems of linear algebraic equations will be formed, and subsequently joined in a single system of linear algebraic equations, by the standard FET assembly process [18].

The systems of linear equations for longitudinal segment currents are obtained using the well-known Galerkin-Bubnov method. Hence, the system of linear equations for longitudinal segment currents, in a matrix notation, can be written as:

$$\left[\bar{Z}^\ell \right] \cdot \left\{ \bar{I}^\ell \right\} = \left[A^\ell \right] \cdot \left\{ \bar{\Phi} \right\} \quad (4)$$

where: $\left[\bar{Z}^\ell \right]$ is a symmetric longitudinal segment impedance matrix, $\left\{ \bar{I}^\ell \right\}$ is a longitudinal segment current vector, $\left\{ \bar{\Phi} \right\}$ is a local nodal potential vector and $\left[A^\ell \right]$ is a two-diagonal longitudinal incidence matrix, with non-zero coefficients described by the following equation:

$$A_{is,is}^\ell = -A_{is,Ns+is}^\ell = 1; \quad is = 1, 2, \dots, Ns \quad (5)$$

Longitudinal self impedance of ks -th segment located in the s -th medium model layer can be computed using the following expression:

$$\bar{Z}_{ks,ks}^\ell = \bar{Z}_{ks}^1 \cdot \ell_{ks} + \bar{f}_{ks,ks} \cdot \frac{j \cdot \omega \cdot \mu_0}{4 \cdot \pi} \cdot \int_{\Gamma_{ks}^s} \int_{\Gamma_{ks}^s} \frac{1}{R} \cdot d\ell_{ks} \ell_{ks}^s \quad (6)$$

where \bar{Z}_{ks}^1 is the internal impedance per unit length of the ks -th segment, ℓ_{ks} is a measure of length along the ks -th segment and $\bar{f}_{ks,ks}$ is the newly-introduced complex attenuation-phase shift factor, defined by (2).

Internal impedance per unit length of the ks -th segment, from (6), is given with the following well-known expression [19]:

$$\bar{Z}_{is}^1 = \frac{\bar{k}}{2 \cdot r_0 \cdot \pi \cdot \sigma_c} \cdot \frac{\bar{J}_0(\bar{k} \cdot r_0)}{\bar{J}_1(\bar{k} \cdot r_0)} \quad (7)$$

where r_0 is the outer radius of the segment, σ_c is the electrical conductivity of the segment material, \bar{J}_0 is the complex Bessel function of the first kind and zero order, \bar{J}_1 is the complex Bessel function of the first kind and first order, while \bar{k} is the complex wave number, defined by the following expression:

$$\bar{k} = \sqrt{\omega \cdot \mu_c \cdot \sigma_c} \cdot e^{-j \cdot \frac{\pi}{4}} \quad (8)$$

where μ_c is the permeability of the segment material. It can be pointed out here that expression (7) needs to be numerically treated with care, due to known inaccuracies which Bessel functions exert for large magnitudes of the function argument (i.e., at high frequencies), [20].

The longitudinal mutual impedance between is -th segment and ks -th segment ($is \neq ks$) can be computed from the following expression:

$$\bar{Z}_{is,ks}^{\ell} = \bar{f}_{is,ks} \cdot \left[\frac{j \cdot \omega \cdot \mu_0}{4 \cdot \pi} \cdot \int_{\Gamma_{is}} \int_{\Gamma_{ks}} \frac{1}{R} \cdot dl_{ks} \cdot dl_{is} \right] \cdot (\vec{\ell}_{0is} \cdot \vec{\ell}_{0ks}) \quad (9)$$

where $\vec{\ell}_{0is}$ and $\vec{\ell}_{0ks}$ are the unit vectors of the segments (Figure 2), while $\bar{f}_{is,ks}$ is again newly-introduced complex attenuation-phase shift factor, defined by Equation (3). The unit vector of the ks -th segment is parallel to the segment axis and oriented from ks to $Ns + ks$ local node.

5. SYSTEM OF LINEAR EQUATIONS FOR TRANSVERSAL SEGMENT CURRENTS

The system of linear equations for transversal segment currents is obtained by again employing the Galerkin - Bubnov method. In matrix notation it can be written as:

$$[\bar{Z}^t] \cdot \{\bar{I}^t\} = [A^t] \cdot \{\bar{\Phi}\} \quad (10)$$

where: $[\bar{Z}^t]$ is a symmetric transversal segment impedance matrix; $\{\bar{I}^t\}$ is a transversal segment current vector; $\{\bar{\Phi}\}$ is a local nodal potential vector as in Equation (4) and $[A^t]$ is again a two-diagonal transversal incidence matrix, with non-zero coefficients now described by the following equation:

$$A_{is,is}^t = A_{is,Ns+is}^t = \frac{1}{2}; \quad is = 1, 2, \dots, Ns \quad (11)$$

In order to determine transversal self and mutual segment impedances in horizontally stratified multilayer medium, two different segment arrangements — in respect to the earth surface — need to be examined, since they involve slightly different approaches.

Theory developed for the time-harmonic current point source in horizontally stratified multilayer medium [11] can be directly applied on horizontal segments, since every point on its axis is positioned at the same depth.

In case of the non-horizontal segments, situation is more difficult. In this case segment axis is not positioned at the same depth. In order to apply the algorithm developed for the time-harmonic current point source, line source along the segment axis has been approximated by five point current sources, each at its own depth. In this case, numerical computation of the integral expression for the time-harmonic current

point source has been carried out with a fivepoint Gauss Legendre quadrature [17]. However, non-horizontal segments are not treated in this paper. Interested reader is advised to consult [16, 17] for more information.

Transversal self impedance of the ks -th horizontal segment, located in the s -th medium model layer, can be written as follows:

$$\bar{Z}_{ks,ks}^t = \bar{f}_{ks,ks} \cdot \left({}^q\bar{Z}_{ks,ks}^t + \sum_{k=2}^{33} \bar{C}_k^{ks} \cdot {}^q\bar{Z}_{ks,k_{ks}}^t \right) \quad (12)$$

where: ${}^q\bar{Z}_{ks,ks}^t$ is a quasistatic transversal self impedance of the ks -th segment in the homogeneous unbounded medium with $\bar{\kappa} = \bar{\kappa}_s$, while ${}^q\bar{Z}_{ks,k_{ks}}^t$ is a quasistatic transversal impedance between the ks -th segment and the k -th image of the ks -th segment in homogeneous unbounded medium, with $\bar{\kappa} = \bar{\kappa}_s$. Here $\bar{f}_{ks,ks}$ again represents the complex attenuation–phase shift factor given by expression (2). Newly introduced value \bar{C}_k^{ks} is a coefficient which defines an intensity of the transversal current for the k -th image of the ks -th segment. These coefficients were originally derived for the current point source positioned in horizontally stratified multilayer medium, by employing the fixed image method, as described in [1, 11].

The quasistatic transversal self and mutual segment impedances in homogeneous unbounded medium with $\bar{\kappa} = \bar{\kappa}_s$, cited in Equation (12), can be respectively computed from the following expressions [16]:

$${}^q\bar{Z}_{ks,ks}^t = \frac{1}{4 \cdot \pi \cdot \bar{\kappa}_s} \cdot \frac{1}{\ell_{ks}^2} \cdot \int_{\Gamma_{ks}^s} \int_{\Gamma_{ks}} \frac{1}{R} \cdot d\ell_{ks} \cdot d\ell_{ks}^s \quad (13)$$

$${}^q\bar{Z}_{ks,k_{ks}}^t = \frac{1}{4 \cdot \pi \cdot \bar{\kappa}_s} \cdot \frac{1}{\ell_{ks}^2} \cdot \int_{\Gamma_{ks}} \int_{\Gamma_{k_{ks}}} \frac{1}{R} \cdot d\ell_{k_{ks}} \cdot d\ell_{ks} \quad (14)$$

Double integrals in Equations (13) and (14) could be analytically solved, which significantly contributes to the numerical efficiency of the electromagnetic model.

According to the model developed for the time-harmonic current point source in horizontally stratified multilayer earth [11], coefficients \bar{C}_1^{ks} , \bar{C}_2^{ks} and \bar{C}_3^{ks} as well as z coordinates of middle point of corresponding segment images (which are obtained by exact image method), are defined according to the following expressions:

$$\bar{C}_1^{ks} = \bar{A}_p \quad (15)$$

$$z_{M1}^{ks} = z_M^{ks} \quad (16)$$

$$\bar{C}_2^{ks} = -\bar{A}_p \cdot \bar{F}_{p-1}; \quad p \leq s; \quad p \neq 1 \quad (17)$$

$$z_{M_2}^{ks} = 2 \cdot H_{p-1} - z_M^{ks}; \quad p \leq s; \quad p \neq 1 \quad (18)$$

$$\bar{C}_2^{ks} = -\bar{A}_p \cdot \bar{F}_{s-1}; \quad p \geq s; \quad s \neq 1 \quad (19)$$

$$z_{M_2}^{ks} = 2 \cdot H_{s-1} - z_M^{ks}; \quad p \geq s; \quad s \neq 1 \quad (20)$$

$$\bar{C}_3^{ks} = \bar{A}_p \cdot \bar{F}_s; \quad p \leq s; \quad s \neq n \quad (21)$$

$$z_{M_3}^{ks} = 2 \cdot H_s - z_M^{ks}; \quad p \leq s; \quad s \neq n \quad (22)$$

$$\bar{C}_3^{ks} = \bar{A}_p \cdot \bar{F}_p; \quad p \geq s; \quad p \neq n \quad (23)$$

$$z_{M_3}^{ks} = 2 \cdot H_p - z_M^{ks}; \quad p \geq s; \quad p \neq n \quad (24)$$

with substitutions $p = s$, $\bar{A}_p = 1$ in the case of Equation (15). The quantity \bar{A}_p in Equations (17), (19), (21) and (23) represents accumulated transmission factor between the s -th and the p -th medium model layers, while quantities \bar{F}_{p-1} , \bar{F}_p , \bar{F}_{s-1} and \bar{F}_s represent associated reflection factors [11].

The coefficients \bar{C}_k^{ks} ; $k = 4, 5, \dots, 33$ and z coordinates of middle point of corresponding segment images are again obtained by fixed image method (applied to point source in horizontally stratified multilayer medium), and could be defined as follows [11]:

$$\bar{C}_k^{ks} = \bar{\alpha}_{k-3}; \quad z_{M_k}^{ks} = H_{p-1} - \vartheta \cdot \eta_{k-3}; \quad k = 4, 5, \dots, 18; \quad p \neq 1 \quad (25)$$

$$\bar{C}_k^{ks} = \bar{\beta}_{k-18}; \quad z_{M_k}^{ks} = H_p + \chi \cdot \eta_{k-18}; \quad k = 19, 20, \dots, 33; \quad p \neq n \quad (26)$$

The coefficients $\bar{\alpha}_k$ and $\bar{\beta}_k$ in (25) and (26) can be computed by an algorithm developed for the time-harmonic current point source located on the ks -th segment axis [11]. The parameters ϑ and χ in Equations (25) and (26) are determined by a set of analytical expressions, based on exact image method [11]. The parameters η in expressions (25) and (26) are chosen on the basis of numerical experiments [16, 17].

If the ks -th segment is horizontal (the is -th segment can be horizontal or non-horizontal), then the transversal mutual impedance between the is -th segment located in the p -th medium model layer and the ks -th segment located in the s -th medium model layer can be computed according to the following expression:

$$\bar{Z}_{is,ks}^t = \bar{f}_{is,ks} \cdot \sum_{k=1}^{33} \bar{C}_k^{ks} \cdot {}^q \bar{Z}_{is,k_{ks}}^t; \quad is \neq ks \quad (27)$$

where: ${}^q \bar{Z}_{is,k_{ks}}^t$ is a quasistatic transversal impedance between the is -th segment and the k -th image of the ks -th segment in the

homogeneous unbounded medium, with $\bar{\kappa} = \bar{\kappa}_p$. All other variables from Equation (27) have been previously defined.

The quasistatic transversal impedance between the is -th segment and the k -th image of the ks -th segment in the homogeneous unbounded medium, with $\bar{\kappa} = \bar{\kappa}_p$, can be computed from the following expression [16]:

$${}^q\bar{Z}_{is, k_{ks}}^t = \frac{1}{4 \cdot \pi \cdot \bar{\kappa}_p} \cdot \frac{1}{\ell_{is} \cdot \ell_{ks}} \cdot \int_{\Gamma_{is}} \int_{\Gamma_{k_{ks}}} \frac{1}{R} \cdot d\ell_{k_{ks}} \cdot d\ell_{is} \quad (28)$$

The double integral in Equation (28) could be again analytically solved. Furthermore, due to the fact that the majority of the above introduced double integrals, involved in expressions for the self and mutual longitudinal and transversal impedances, have known analytical solution, here presented algorithm becomes very numerically efficient. This is in turn due to the introduction of the attenuation-phase shift factors, which circumvent the need for the time-consuming numerical solution of Sommerfeld integrals.

6. GLOBAL SYSTEM OF LINEAR ALGEBRAIC EQUATIONS

In the global system, segments are connected in global nodes, according to the FET terminology [18]. For a set of connected segments in multilayer medium, the global system of linear algebraic equations can be written as follows [18]:

$$[\bar{Y}_g] \cdot \{\bar{\Phi}_g\} = \{\bar{I}_g\} \quad (29)$$

where: $[\bar{Y}_g]$ is a global system admittance matrix (global nodal admittance matrix); $\{\bar{\Phi}_g\}$ is an unknown global nodal potential vector and $\{\bar{I}_g\}$ is a known global nodal current vector formed from the currents applied on the conductors under consideration.

The assembly process on the local system admittance matrices produces a global system admittance matrix. This is a standard FET procedure [18]. The associated longitudinal and transversal local system admittance matrices can be respectively written as follows:

$$[\bar{Y}^\ell] = [A^\ell]^T \cdot [\bar{Z}^\ell]^{-1} \cdot [A^\ell] \quad (30)$$

$$[\bar{Y}^t] = [A^t]^T \cdot [\bar{Z}^t]^{-1} \cdot [A^t] \quad (31)$$

The global nodal potentials are obtained by solving the system of linear algebraic Equation (29). Once the global nodal

potentials become known, the local nodal potentials are obtained straightforwardly, through the application of the incidence vector used in the assembly process. Now, one can compute longitudinal and transversal nodal currents, using the following matrix equations:

$$\{\bar{I}^{nl}\} = [\bar{Y}^\ell] \cdot \{\bar{\Phi}\} \quad (32)$$

$$\{\bar{I}^{nt}\} = [\bar{Y}^t] \cdot \{\bar{\Phi}\} \quad (33)$$

These nodal currents are needed in computation of the longitudinal and transversal segment currents. Connection between longitudinal and transversal nodal currents and segment currents could be expressed with the following matrix equations:

$$\{\bar{I}^\ell\} = \left([A^\ell]^T \right)^{-1} \cdot \{\bar{I}^{nl}\} \quad (34)$$

$$\{\bar{I}^t\} = \left([A^t]^T \right)^{-1} \cdot \{\bar{I}^{nt}\} \quad (35)$$

Once the current distribution on the segments (i.e., conductor grid) has been obtained, one can proceed with the computation of potential distribution, as well as distribution of the electric and magnetic field intensities. Hence, a first step in the solution procedure for the system of conductors in horizontally stratified multilayer medium is the above presented computation of the current distribution on those same conductors. A numerically efficient solution is here obtained from the equally efficient solution of the potential distribution, in the same multilayer medium, due to time-harmonic current point source [11].

7. MODEL VALIDATION

Model validation will be carried out through the comparison of the results obtained with here presented electromagnetic model with those obtained by other state-of-the-art so-called full-wave electromagnetic model. Hence, current distribution on the segments buried in two-layer soil is computed and compared with results obtained with a full-wave electromagnetic model, developed for the two-layer soil [8, 9]. Model presented in [8, 9], constitutes an extension of the sophisticated model presented in [5], and rigorously treats layer boundaries, by numerically solving associated Sommerfeld integrals.

Here treated numerical example has been obtained from [8], with the same geometry, conductor properties, soil properties and disposition. This example firstly features a single 5 mm radius horizontal copper conductor, buried at 0.75 m depth in a two-layer

soil, as depicted in Figure 3. Length of the conductor equals 10 m. Characteristics of the soil layers are varied as explained in [8] and presented in Table 1. It can be seen from Table 1 that two scenarios have been treated (Case 1 and Case 2), each with two additional variants (a and b).

Table 1 also illustrates the variation of the position of conductor in the upper or bottom layers of the two-layer soil, which is achieved by changing the depth of the first soil layer. It is hereafter assumed that permittivity of both soil layers equals 10 in all treated examples, as has been the case in [8].

Current of $1 + j0$ A is injected into its one end, as depicted in Figure 3. Distribution of the current along this 10 m long conductor for frequencies: 0.1 MHz, 1 MHz and 10 MHz, for every combination of conductor position (first or second soil layer) and every combination of soil parameters from Table 1 is hereafter presented. This is in accordance with the treatment carried out in [8].

Figure 4 presents a current magnitude distribution along the 10 m long horizontal conductor at frequency of 0.1 MHz, for every combination of conductor position and every combination of soil parameters given in Table 1. Very little difference in current distribution could be observed from Figure 4. This is in accordance with conclusions derived in [8].

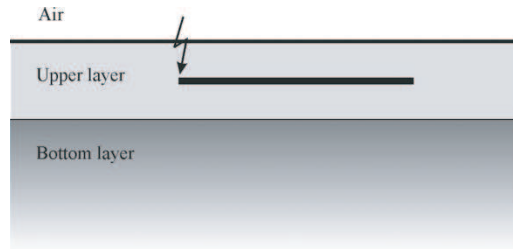


Figure 3. Single horizontal segment in two-layer soil.

Table 1. Parameters of both layers used in the analysis.

	Upper layer depth (m)	Upper layer ρ (Ωm)	Bottom layer ρ (Ωm)
Case 1	1.0	100	a) 1000
			b) 10
Case 2	0.5	a) 1000	100
		b) 10	

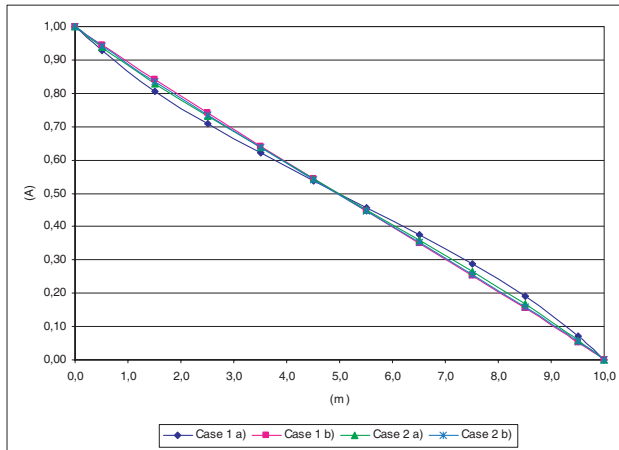


Figure 4. Current distribution along 10 m long conductor at 0.1 MHz, for every combination of soil parameters from Table 1.

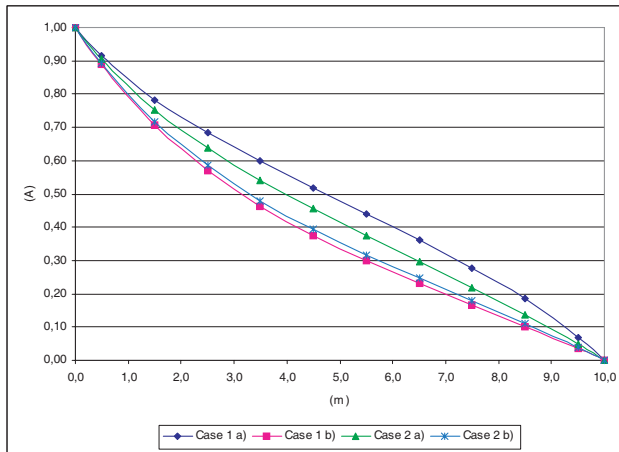


Figure 5. Current distribution along conductor at 1 MHz, for every combination of soil parameters from Table 1.

Figures 5 and 6, at the same time, present current magnitude distribution along this 10 m long horizontal conductor at frequency of 1 MHz and 10 MHz, respectively. Current distributions are again given for every combination of conductor position and soil parameters, according to the data presented in Table 1.

By comparing Figures 4, 5 and 6 with those presented in [8], very good agreement could be observed at every considered frequency up to

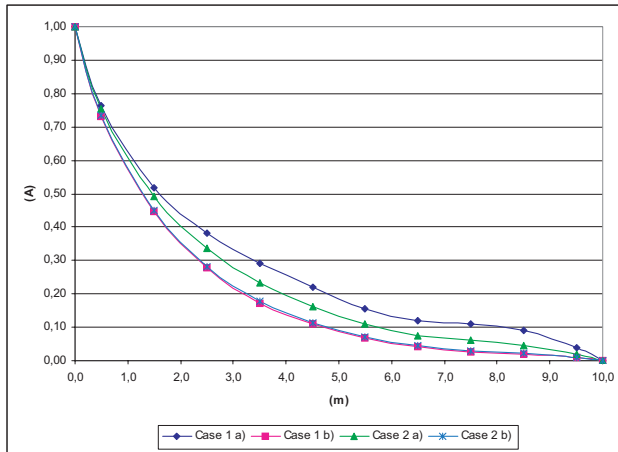


Figure 6. Current distribution along 10 m conductor at 10 MHz, for every combination of soil parameters from Table 1.

10 MHz, in all treated soil parameter combinations.

Furthermore, impedance to ground of this 10 m long conductor has been computed as well, for several different frequencies, ranging up to 10 MHz. Obtained results are presented in Table 2. Again, good agreement between results from Table 2 and those presented in [8] could be established, for the entire considered frequency range.

It can be appreciated from the Table 2 that, in the low frequency range, impedance to ground is almost frequency independent. It is highly dependent on soil parameters of both soil layers. Influence of neighboring layer parameters on impedance is especially strong in this lower frequency range. On the other hand, in the high frequency range, impedance becomes very frequency dependent. At the same time, its dependence on both soil layer parameters weakens. This behavior is in accordance with previously published work and conclusions derived in [8].

Comparison of results presented in Table 2 with those published in [8] reveals that the maximum error in the computed impedance exists for the Case 1a). The estimated relative error for this case amounts to 9% at the frequency of 1 MHz, and it grows to 15% at the 10 MHz. For all other treated cases the relative errors are lower. As far as the duration of the numerical computation is concerned, it is extremely short for the treated cases. It amounts to under one second for each of the treated cases. Hence, considering the errors inherent in the interpretation of geoelectrical sounding data, compounded by the errors in soil resistivity measurements (exacerbated by the

Table 2. Impedance to ground of grounding conductor.

	Impedance (Ω)			
	10 kHz	100 kHz	1 MHz	10 MHz
Case 1 a)	33.8	30.9	32.3	67.1
Case 1 b)	8.2	8.8	23.9	61.1
Case 2 a)	15.4	15.8	28.9	67.8
Case 2 b)	10.6	10.8	25.1	62.4

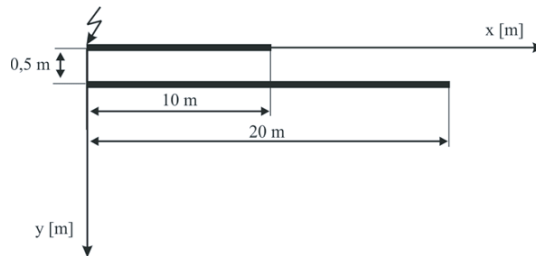


Figure 7. Disposition of energized and near-by passive conductor.

seasonal variations of soil parameters), this would seem satisfactory. Moreover, the trade-of between the computation speed (obtained from this approach) and its accuracy is well balanced.

Additionally, in order to demonstrate a complete electromagnetic coupling between grounding grid conductors, a new passive near-by copper conductor has been placed at 0.75 m depth and 0.5 m apart from the initially treated conductor. This new passive near-by conductor is assumed to be 20 m long [8]. Disposition (top view) of energized and passive near-by conductor is graphically illustrated in Figure 7.

It can be seen from Figure 7 that conductors are parallel to each other, buried at the same depth and in horizontal position, relative to the earth surface. Near-by conductor has a 5 mm radius as well. In order to demonstrate the electromagnetic coupling between segments, current distribution along this passive near-by conductor is computed, for various frequencies and soil parameters.

Figure 8 presents a current magnitude distribution along the passive near-by 20 m long horizontal conductor at frequency of 0.1 MHz, while Figure 9 at the same time presents the same distribution but at frequency of 1 MHz. Current magnitude distributions from Figures 8 and 9 are given for every combination of conductor positions (both conductors in upper or lower soil layer) and every combination of soil parameters, according to data presented in Table 1 [8].

By comparing Figures 8 and 9 with those presented in [8], a very good agreement could be again observed, for every considered frequency and soil parameters combination from Table 1.

Hence, it can be stated that here developed electromagnetic model for determining the current distribution on system of conductors (i.e., conductor grid) in horizontally stratified multilayer medium could be

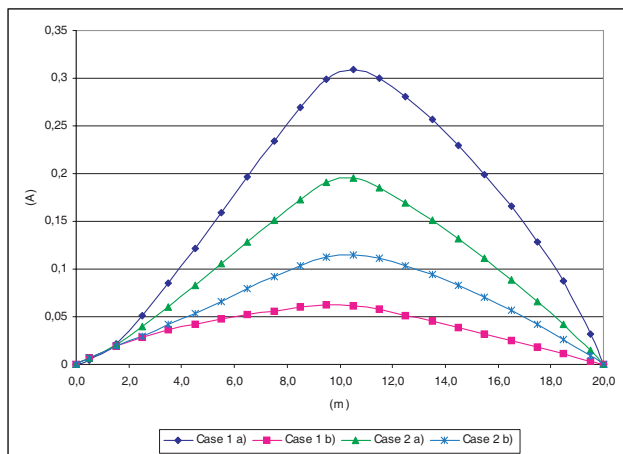


Figure 8. Current distribution along 20 m passive near-by conductor at 0.1 MHz, for every combination of soil parameters from Table 1.

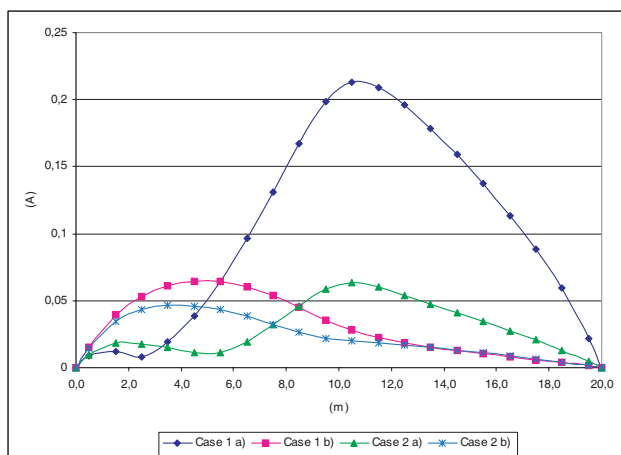


Figure 9. Current distribution along 20 m passive near-by conductor at 1 MHz, for every combination of soil parameters from Table 1.

successfully applied in the mentioned frequency range. This frequency range is in-turn often associated with the first negative lightning stroke currents [21].

8. CONCLUSION

This paper presented a novel time-harmonic electromagnetic model for determining the current distribution on conductor grid in horizontally stratified multilayer medium. This model could be seen as a cornerstone of the wider electromagnetic model for the frequency-domain transient analysis of conductor grid in horizontally stratified multilayer medium. Complete electromagnetic coupling between conductor segments has been taken into account. Numerical solution of Sommerfeld integrals has been avoided through an approximation of the attenuation and phase shift effects. This fact, along with the fact that majority of integrals involved in computation of the self and mutual impedances could be analytically solved, has assured a high numerical efficiency of the presented model.

It should be accentuated that here presented electromagnetic model straightforwardly interconnects segments at their connection points, which is due to the application of the assembly procedure of the finite element technique. Hence, parallel and perpendicular segments are equally treated, which is not the case in other methods (i.e., there is no need for overlapping of segments in their connecting points). Furthermore, extension from the single conductor case (or a two-conductor system) to the full conductor grid, with arbitrary number and position of conductors, is a straightforward task.

Validation of the here developed model is carried out with comparison of results with those obtained by a full-wave electromagnetic model, developed for the two-layer soil. Very good agreement between results presented here and those obtained with a full-wave model has been found, in various examples of two-layer soil model parameters and at various treated frequencies. This in fact acknowledges an important part of the frequency range in which the here presented electromagnetic model could be applied.

Future research on this electromagnetic model will pursue the implementation of the Fourier transform for its extension into the frequency-domain transient analysis. Furthermore, determination of the potential distribution, as well as the electromagnetic field distribution, due to energized system of conductors in horizontally stratified multilayer medium will be pursued.

REFERENCES

1. Sarajčev, P. and S. Vujević, "Grounding grid analysis: Historical background and classification of methods," *International Review of Electrical Engineering*, Vol. 4, No. 4, 670–683, 2009.
2. Berberovic, S. and V. Boras, "Modified numerical current field calculation in determining non-equipotential large earthing system parameters," *Proc. of the 25th Int. Conf. on Lightning Protection*, 478–483, Rhodes, Greece, 2000.
3. Boras, V., S. Berberovic, and S. Nikolovski, "Improved numerical calculation of earthing system parameters in non-equipotential AC substation earthing grids," *Proc. of the 26th Int. Conf. on Lightning Protection*, 388–393, Cracow, Poland, 2002.
4. Otero, A. F., J. Cidras, and J. L. Del Alamo, "Frequency-dependent grounding system calculation by means of a conventional nodal analysis technique," *IEEE Transactions on Power Delivery*, Vol. 14, No. 3, 873–878, 1999.
5. Grcev, L. and F. Dawalibi, "An electromagnetic model for transients in grounding systems," *IEEE Transactions on Power Delivery*, Vol. 5, No. 4, 1773–1781, 1990.
6. Dawalibi, F., "Electromagnetic fields generated by overhead and buried short conductors, Part I — Single conductor," *IEEE Transactions on Power Delivery*, Vol. 1, No. 4, 105–111, 1986.
7. Dawalibi, F., "Electromagnetic fields generated by overhead and buried short conductors, Part II — Ground networks," *IEEE Transactions on Power Delivery*, Vol. 1, No. 4, 112–119, 1986.
8. Arnautovski-Toševa, V., L. Grčev, and K. El Khamlichi Drissi, "High frequency electromagnetic analysis of horizontal earthing conductor and near-by passive parallel conductor within two-layer soil," *15 International Conference on Software Telecommunications and Computer Network, (SoftCOM 2007)*, Split, Croatia, Sep. 27–29, 2007.
9. Arnautovski-Toševa, V. and L. Grčev, "Electromagnetic analysis of horizontal wire in two-layered soil," *Journal of Computational and Applied Mathematics*, Vol. 168, No. 1–2, 21–29, 2004.
10. Li, Z.-X., W. Chen, J. B. Fan, and J. Lu, "A novel mathematical modeling of grounding system buried in multilayer earth," *IEEE Transactions on Power Delivery*, Vol. 21, No. 3, 1267–1272, 2006.
11. Vujević, S. and P. Sarajčev, "Potential distribution for a harmonic current point source in horizontally stratified multilayer medium," *The International Journal for Computation and Mathematics in Electrical and Electronic Engineering (COMPEL)*, Vol. 27, No. 3,

- 624–637, 2008.
12. Grcev, L. and V. Arnautovski-Toseva, “Grounding systems modeling for high frequencies and transients: Some fundamental considerations,” *2003 IEEE Bologna Power Tech Conference*, Bologna, Italy, Jun. 23–26, 2003.
 13. Visacro, S. and G. Rosado, “Response of grounding electrodes to impulsive currents: An experimental evaluation,” *IEEE Transactions on Electromagnetic Compatibility*, Vol. 1, No. 1, 161–164, 2009.
 14. Stojkovic, Z., M. S. Savic, J. M. Nahman, D. Salamon, and B. Bukorovic, “Sensitivity analysis of experimentally determined grounding grid impulse characteristics,” *IEEE Transactions on Power Delivery*, Vol. 13, No. 4, 1136–1142, 1998.
 15. Sekioka, S., H. Hayashida, T. Hara, and A. Ametani, “Measurements of grounding resistances for high impulse currents,” *IEE Proceedings — Generation, Transmission and Distribution*, Vol. 145, No. 6, 693–699, 1998.
 16. Vujević, S. and M. Kurtović, “Numerical analysis of earthing grids buried in horizontally stratified multilayer earth,” *International Journal for Numerical Methods in Engineering*, Vol. 41, 1297–1319, 1998.
 17. Vujević, S., P. Sarajčev, and R. Lucić, “Computing the mutual impedances between segments of earthing system conductors,” *Computational Methods and Experimental Measurements XII*, 641–650, WIT Press, Southampton, UK, 2005.
 18. Silvester, P. P. and R. L. Ferrari, *Finite Elements for Electrical Engineers*, 3rd edition, Cambridge University Press, Cambridge, 1996.
 19. Vujević, S., V. Boras, and P. Sarajcev, “A novel algorithm for internal impedance computation of solid and tubular cylindrical conductors,” *International Review of Electrical Engineering (IREE)*, Vol. 4, No. 6, 1418–1425, 2009.
 20. Lovrić, D., V. Boras, and S. Vujević, “Accuracy of approximate formulas for internal impedance of tubular cylindrical conductors for large parameters,” *Progress In Electromagnetics Research M*, Vol. 16, 177–184, 2011.
 21. Grcev, L., “Impulse efficiency of ground electrodes,” *IEEE Transactions on Power Delivery*, Vol. 24, No. 1, 441–451, 2009.